

# Simulations of Swaying Effect of Coastal Vegetation on Tsunami Damping

Ching-Piao Tsai<sup>1</sup>, Ying-Chi Chen<sup>1</sup>, Tri Octaviani Sihombing<sup>2</sup> and Chang Lin<sup>1</sup>

<sup>1</sup>Department of Civil Engineering, National Chung Hsing University, Taichung 402, Taiwan

5 <sup>2</sup>Department of Civil Engineering, Maranatha Christian University, Bandung 40164, Indonesia

*Correspondence to:* Ching-Piao Tsai (cptsai@nchu.edu.tw)

**Abstract.** A coupled wave-vegetation simulation is presented for the swaying effect of the coastal vegetation on tsunami wave height damping. The problem is idealized by solitary wave propagating on a group of emergent cylinders. The numerical model is based on general Reynolds-averaged Navier-Stokes equations with renormalization group turbulent closure model by using volume of fluid technique. The general moving object (GMO) model developed in CFD code Flow-3D is applied to simulate the coupled motion of vegetation with wave dynamically. The damping of wave height and the turbulent kinetic energy as waves passed over both swaying and stationary cylinders are discussed. The simulated results show that the damping of wave height and turbulent kinetic energy by the swaying cylinders were markedly less than by the stationary cylinders. The result implies that the wave decay by the coastal vegetation might be overestimated if the mangrove  
10  
15 vegetation was represented as stationary state.

## 1 Introduction

A huge tsunami in South East Asia caused catastrophic damage and claimed more than 200,000 people in December 2004. Cochard et al. (2008) pointed out that this event has stimulated a debate about the role played coastal ecosystems such as mangrove forests and coral reefs in protecting low-lying coastal area. For example, Baird (2006) questioned the effectiveness  
20 of the coastal forests or reefs on the reduction of the damage caused by the tsunami. However, Danielsen et al. (2005) reported areas with coastal tree vegetation were markedly less damaged than areas without. Iverson and Prasad (2007) also indicated that developed areas were far more likely to be damaged than forested zones. Several studies (Hiraishi and Harada, 2003; Harada and Kawata, 2004; Teh et al., 2009) have shown that tsunami wave energy, heights and velocities were significantly reduced as the wave propagates through mangrove forests. Nevertheless, Wolanski (2006) has noted that  
25 mangroves probably cannot protect the coast against a tsunami wave greater than a threshold level based on some evidence from observations of the Indian Ocean tsunami. **Based on the field observations, Shuto (1987) and Yanagisawa et al. (2009) found that single trees or even entire forests could be destroyed through tilting, uprooting, bending or trunk breaking by**

**tsunami.** For tsunami being always present a threat to lives and property along the most coasts of the world, it remains an important for estimating the effectiveness of the coastal vegetation on the tsunami impact.

Many numerical and experimental approaches have been developed in recent years to help understanding the tsunami wave interactions with coastal vegetation. The coastal **tree** vegetation was idealized by a group of rigid cylinders in most investigations. Huang et al. (2011) performed both experiments and a numerical model by considering solitary wave propagating on emergent rigid cylinders and found that dense cylinders may reduce the wave transmission because of the increased wave energy dissipation into turbulence in cylinders. By using both direct numerical simulation and macroscopic approach, Maza et al. (2015) simulated the interaction of solitary waves with emergent rigid cylinders based on the arrangement of laboratory experiments of Huang et al. (2011). Previous approaches (e.g. Anderson et al., 2011; Huang et al., 2011; Maza et al., 2015; Wu et al., 2016) assumed that the idealized mangrove vegetation is stationary and neglected the plant motion with the wave.

There are several works investigated the hydraulic resistance of coastal vegetation involving the flexible effect of plants. Zhang et al. (2015) pointed out that the prop roots under tidal hydrodynamic loadings in a mangrove environment can be regarded as fairly rigid on account of a large Young's modulus. However, Augustin et al. (2009) indicated that motion of the flexible elements is an important factor on wave attenuation based on flume tests considering both stiff and flexible parameterised tree models under wave action. Husrin (2013) investigated that the trunk of mangrove with its strength properties may behave as a stiff or flexible structure which also governs its relative contribution to the total energy dissipation under tsunami and storm wave action. Coastal pines, one of typical coastal forest vegetation have longer trunk compared to mangroves, Husrin and Oumeraci (2013) indicated that they are more deflected when subject to similar flow velocity compared to mangroves. Husrin et al. (2012) and Strusińska et al. (2013; 2014) examined the tsunami attenuation by coastal vegetation under laboratory conditions for mature mangroves using parameterized trees including flexible tree models. Maza et al. (2013) presented a new numerical model for the interaction of wave and flexible swaying vegetation which couples the flow and the plant motion considering the plant deformation using RANS equation with  $k-\varepsilon$  turbulent model.

Some mangrove roots and branches at the stage of growing are hanging from the canopy to the flow; it causes the prop roots to oscillate in the water. This study presents the numerical simulation considering vegetation motion coupled with tsunami waves to investigate the wave damping performance. Similar to the experimental work of Kazemi et al. (2015), we model the swaying motion of the vegetation by attaching rigid cylinders to torsional connectors under wave action. This is also a simplified way to represent some movements of mangroves induced by sediment scour, tilting or uprooting states. A direct numerical model based on computational fluid dynamics (CFD) is presented in this paper for simulating the wave damping characteristics including both stationary and swaying vegetation.

## 2 Numerical model description

Among a number of open source CFD codes available, **IHFOAM** (Higuera et al., 2013; 2014) is specially designed for coastal engineering applications. **IHFOAM** model was used in Maza et al. (2015) for direct numerical simulation of the solitary wave interacting with the stationary vegetation. Alternatively, the model Flow-3D (Flow Science, Inc., 2012) is applied in this paper to conduct the numerical simulations **including vegetation motion under wave action**. Flow-3D provides exclusively the FAVOR (fractional area/volumes obstacle representation) technique (Hirt, 1993) and the general moving object (GMO) model that is capable of simulating the rigid body motion dynamically coupled with fluid flow. The FAVOR technique retains rectangular elements with a simple Cartesian grid system and **has been** shown to be one of the most efficient methods to treat the immersed solid bodies (Xiao, 1999). The free water surface tracking in the model is accomplished by using volume of fluid (VOF) method (Hirt and Nichols, 1981).

Referring to previous literature, the problem is idealized by solitary wave passing on a group of emergent rigid cylinders. Considering the fluid to be incompressible, the continuity and momentum equations for a moving object formulated with area and volume fraction functions are given as

$$\frac{\partial(u_i A_i)}{\partial x_i} = -\frac{\partial V_F}{\partial t}, \quad (1)$$

$$\frac{\partial u_i}{\partial t} + \frac{A_j u_j}{V_F} \frac{\partial u_i}{\partial x_j} = -\frac{1}{\rho} \frac{\partial p}{\partial x_i} + g_i + \frac{1}{\rho V_F} \frac{\partial}{\partial x_j} \left[ 2A_j [(\mu + \rho \nu_t) S_{ij} - \frac{2}{3} \rho k \delta_{ij}] \right] \quad (2)$$

where  $S_{ij} = (\partial u_i / \partial x_j + \partial u_j / \partial x_i) / 2$ ,  $V_F$  is the fractional volume open to the flow, and  $A_j$  is the fraction area for the subscript direction, the subscripts of  $i$  and  $j = 1, 2, 3$  represent  $x$ -,  $y$ - and  $z$ - directions,  $x_i$  and  $x_j$  represent Cartesian coordinates,  $u_i$  and  $u_j$  are the mean velocity component in subscript direction,  $t$  is the time,  $p$  is the pressure intensity,  $\rho$  is the fluid density,  $g$  is the gravitational acceleration,  $\mu$  is the absolute viscosity,  $\nu_t$  is the eddy viscosity,  $k$  is the turbulent kinetic energy, and  $\delta_{ij}$  is the Kronecker delta function such that  $\delta_{ij} = 1$  when  $i = j$ ;  $\delta_{ij} = 0$ , when  $i \neq j$ . It is noted that the above governing equations are rendered to standard RANS equations as both  $V_F$  and  $A$  are set to unity.

The eddy viscosity  $\nu_t$  in Eq. (2) takes the form as

$$\nu_t = c_\mu \frac{k^2}{\varepsilon} \quad (3)$$

where  $k$  and  $\varepsilon$  represent the turbulent kinetic energy and turbulent energy dissipation rate, respectively.  $k$  and  $\varepsilon$  are related to the effect of space and time distribution of the turbulent motion, which can be solved by a variety of turbulent closure models including one equation model, two equations  $k$ - $\varepsilon$  model, Renormalization Group method (RNG  $k$ - $\varepsilon$  model), Large Eddy Simulation (LES), and Shear Stress Transport ( $k$ - $\omega$  SST) model etc. The RNG  $k$ - $\varepsilon$  turbulent model was originally

derived by Yokhot and Orszag (1986) based on Renormalization Group methods and improved by Yakhot et al. (1992) with scale expansions for the Reynolds stress and production of dissipation terms. The RNG  $k$ - $\varepsilon$  model can be a useful turbulence model for practical engineering and scientific calculations (Speziale and Thangam, 1992). Choi et al. (2007) applied RNG  $k$ - $\varepsilon$  turbulent model to the three-dimensional simulation of tsunami run-up around conical island and demonstrated that it is with computational efficiency and accuracy. RNG  $k$ - $\varepsilon$  turbulent model has been proved having reliability for a wider class of flows, thus it is selected to apply in this paper.

Referring to Yakhot et al. (1992), the turbulent transport equations of the RNG  $k$ - $\varepsilon$  model are expressed as

$$\frac{\partial k}{\partial t} + \frac{u_i A_i}{V_F} \frac{\partial k}{\partial x_i} = P - \varepsilon + \frac{1}{V_F} \frac{\partial}{\partial x_i} \left( \frac{\nu_t A_i}{\sigma_k} \frac{\partial k}{\partial x_i} \right) \quad (4)$$

$$\frac{\partial \varepsilon}{\partial t} + \frac{u_i A_i}{V_F} \frac{\partial \varepsilon}{\partial x_i} = c_{\varepsilon 1} \frac{\varepsilon}{k} P - c_{\varepsilon 2} \frac{\varepsilon^2}{k} + \frac{1}{V_F} \frac{\partial}{\partial x_i} \left( \frac{\nu_t A_i}{\sigma_\varepsilon} \frac{\partial \varepsilon}{\partial x_i} \right) \quad (5)$$

where  $P$  is the turbulence kinetic energy production given by

$$P = 2\nu_t S_{ij} \hat{S}_{ij}, \quad \hat{S}_{ij} = \frac{1}{V_F} \left( A_j \frac{\partial u_i}{\partial x_j} + A_i \frac{\partial u_j}{\partial x_i} \right) \quad (6)$$

The coefficients are summarized as follows:

$$C_\mu = 0.085, \quad C_{\varepsilon 1} = 1.42 - \frac{\alpha(1 - \alpha / \alpha_o)}{1 + \beta \alpha^3} \quad (7)$$

$$C_{\varepsilon 2} = 1.68, \quad \sigma_k = 0.7179, \quad \sigma_\varepsilon = 0.7179$$

where  $\alpha = Sk / \varepsilon$ ,  $S = (2S_{ij} \hat{S}_{ij})^{1/2}$ ,  $\alpha_o = 4.38$ ,  $\beta = 0.015$ .

For coupling the rigid body motion dynamically with fluid flow, the general moving object (GMO) model is adopted here. Comparing with the continuity equation for stationary obstacle problems,  $-\partial V_F / \partial t$  in equation (1) is equivalent to an additional volume source term and exists only in mesh cells around the moving object boundary. It can be calculated using

$$-\frac{\partial V_F}{\partial t} = \frac{S_{obj}}{V_{cell}} u_{obj} n_j \quad (8)$$

where  $V_{cell}$  is volume of a mesh cell,  $S_{obj}$ ,  $n_j$  and  $u_{obj}$  are respectively surface area, unit normal vector and velocity of the moving object in the mesh cell. The relative transport equation for the VOF function  $F$  is given using

$$\frac{\partial F}{\partial t} + \frac{1}{V_F} \frac{\partial (F u_i A_i)}{\partial x_i} = -\frac{F}{V_F} \frac{\partial V_F}{\partial t} \quad (9)$$

According to kinematics, general motion of a rigid body can be divided into a translational motion and a rotational motion.

If the cylinder is considered to sway in the  $x$ -direction accompanied by wave, angular velocity of the swaying cylinder is the only one non-zero component. Then the equations of motion of the cylinder are rendered as

$$T = J\dot{\omega} \quad (10)$$

where  $T$ ,  $J$ , and  $\dot{\omega}$  are total torque, moment of inertia and angular acceleration about the fixed axis. And the velocity of any point G on the swaying cylinder is calculated by  $V_G = \omega r_{G/C}$ , where  $r_{G/C}$  denotes distance from the fixed end C of the cylinder to point G.

In computing the coupling of fluid and rigid body interaction, the velocity and pressure of fluid flow are first solved. The hydrodynamics forces on the rigid body are then obtained and used to calculate the velocity of the rigid body. Then the volume and area fractions are updated according to the new position of the rigid body, and the source term can be calculated using equation (8). The flow field is computed repeatedly until the convergence is achieved. **The similar GMO model was well applied for the numerical simulation of the coupled motion of solid body and waves, e.g. Bhinder et al. (2009), Dental et al. (2014), and Zhao et al. (2014).**

As for the boundary conditions for solving the governing equations of flow, the normal stress is in equilibrium with the atmospheric pressure while shearing stress is zero on the free surface. All of the solid surfaces were treated using the no-slip boundary condition. The variation of the turbulent energy and the turbulent energy dissipation on the free surface boundary was set as zero in the normal direction. The solution of solitary wave derived from Boussinesq equations was employed as the incident wave.

### 3 Validation

Huang *et al.* (2011) conducted laboratory experiments in a wave flume for the solitary waves interacting with emergent, rigid vegetation. The vegetation was considered as a group of cylinders which were made of Perplex tubes with a uniform outer diameter of 0.01 m. The computations used the same geometric configuration of Huang's laboratory works. The water depth was uniform and equal to  $h = 0.15$  m, and the cylinder height was 0.24 m. **The arrangement of cylinders shown in Fig. 1 was selected to validate the present numerical simulation. Examples of two vegetation lengths,  $L = 1.635$  m and 0.545 m, shown in previous studies are simulated here.** The numerical tank was set by 6 m long, 0.55 m wide and 0.3 m height. Note that the verification of the model performance is only implemented by the case of stationary cylinders because the experimental information on the swaying cylinders by solitary waves is unfortunately lacking.

Two different uniform computational meshes around the cylinder field, 0.002 m and 0.001 m respectively, were used to test the numerical accuracy and the sensitivity to grid size. Fig. 2 shows that FAVOR technique resolved successfully the geometry of cylinders using these two computational grids constructed. **It indicates that the FAVOR efficiently uses 29 and 17 points to define each cylinder for the mesh of  $0.001 \text{ m} \times 0.001 \text{ m}$  and  $0.002 \text{ m} \times 0.002 \text{ m}$ , respectively.**

Fig. 3 shows the comparison of free surface evolution between the present numerical results and experimental measurements for an incident wave height  $H_i = 0.05$  m **considering the vegetation length  $L = 1.635$  m.** The results obtained

by the direct simulation using IHFOAM with  $k-\omega$  SST turbulent model in Maza *et al.* (2015) were also shown in the figure. The comparisons depict that the present numerical results are in a good agreement with the laboratory experiments and previous numerical simulations. The second validation is performed by considering the vegetation length  $L = 0.545$  m to compare with the Fig. 14 of Maza *et al.* (2015) using  $H_i = 0.05$  m. The simulated result of wave height evolution shown in Fig. 4 depicts in a good agreement with previous numerical results, though the present simulation used different turbulent model. The comparisons shown in Figs. 3 and 4 also demonstrate that there are almost no differences between both computational meshes for the free surface or wave height evolution.

## 4 Results and discussion

The above comparisons demonstrated the present numerical model is capable of simulating accurately the wave evolution by the group cylinders. The following simulations are performed for solitary wave passing through both the stationary and swaying cylinders. The surface elevation evolution, flow field variation, and the turbulent kinetic energy are analysed and compared between both stationary and swaying cylinders. The numerical domain and the arrangement of cylinders used in the following simulations are the same as in previous section. The fine mesh with 0.001 m is used for the following computations.

The swaying cylinders induced by waves are set-up by the general moving object (GMO) model for coupling the cylinder's motion and fluid flow dynamically. Similar to Kazemi *et al.* (2015), each cylinder end was simplified by attaching a torsion spring connector on the bottom in the model. The use of torsion spring could not completely reproduce the natural bending behaviour of the mangrove tree, but it allows the cylinders to swaying with the passing wave. Peltola *et al.* (2000) and Husrin (2013) indicated that the deflection angles for a broken trunk may range from  $23^\circ$  to  $42^\circ$ . Too higher value of the specific gravity and lower spring constant used in the present model scale will produce too larger deflection angle of the cylinders and no longer with elastic behaviour. Accordingly, after many numerical tests, the spring constants are set by values of  $k_s = 1 - 1.8$  kgw/m with the cylinder's specific gravity of 0.25 to affirm that cylinders can return back to their original position after being hit by waves.

### 4.1 Free surface evolution

The numerical free surface evolutions for the swaying and stationary cylinders respectively are shown in Fig. 5. The spring constant is set by  $k_s = 1.0$  kgw/m in this case. It can be seen that the free surface elevation decays rapidly along the cylinder array by stationary cylinders but mildly by swaying cylinders.

Fig. 6 shows the comparison of wave height evolution for swaying cylinders with different spring constants, which can be seen that the results of swaying and stationary cylinders are almost identical for  $k_s = 1.8$ . Besides, Fig. 7 shows that the larger spring constants the larger maximum deflection angle is. It also shows that the front rows of cylinders get larger deflection. It is noted that the spring constant  $k_s = 1.0$  kgw/m is used in the following examples.

Fig. 8 shows the variation of the wave height damping ratio,  $H_D = (H - H_i) / H_i$ , along the cylinder array for different incident wave heights. It can be seen that the maximum wave height damping ratio of  $H_i/H = 0.33$  is approximately 26% for swaying cylinders but it could reach to 61% for stationary cylinders. The result of free surface evolution depicts that the stationary cylinders are working better than the swaying cylinders for the wave height damping. That is, the wave height decay can be overestimated if the coastal vegetation was considered as stationary state.

#### 4.2 Flow field evolution

Fig. 9 shows the snapshots of velocity distribution at the centre line of the tank for swaying and stationary cylinders as the solitary wave crest is passing through gauges G3 to G6 for an incident wave height  $H_i = 0.05$  m. It can be observed that the water velocity reduces rapidly along the array of stationary cylinders, but it reduces gently by swaying cylinders. The swaying cylinders have angular motion and even become immerse in the water under the wave crest, thus it leads to the flow velocity be larger than that of stationary cylinders. Fig. 10 shows the comparison of the horizontal velocity profile as wave crest is passing through gauges G3 to G6, i.e.  $x/L = 0, 0.33, 0.66$  and  $1.0$ , for swaying and stationary cylinders. It can be seen that the profiles vary oscillatory for swaying cylinders due to the motion effect of cylinder.

#### 4.3 Turbulent kinetic energy evolution

The turbulent kinetic energy will be generated and dissipated during the wave interacting with the group of cylinders. The turbulent kinetic energy ( $k$ ) and the turbulent kinetic energy dissipation rate ( $\varepsilon$ ) are obtained from the RNG  $k-\varepsilon$  turbulent closure model while the general RANS equations is solving. We focus on when and where the maximum turbulent kinetic energy occurs for an incident wave height  $H_i = 0.05$  m.

Figs. 11 and 12 display the snapshots of the spatial distribution of the turbulent kinetic energy (TKE) and the turbulent kinetic energy dissipation rate (DTKE) for swaying and stationary cylinders, respectively, when the wave crest is passing through gauges G3 to G6. It shows that the turbulent kinetic energy start generating and dissipating as the wave crest is hitting on the front row of cylinders. It can be seen that the characteristics of spatial distribution of TKE and DTKE for swaying and stationary cylinders are very similar. Figs. 13 and 14 display the time variations of TKE at each section ( $x/L = 0 - 1$ ), which shows that the maximum TKE occurs at  $x/L = 0.33$  of both cylinders. The result can be stated that the maximum TKE is not occurring when the wave crest is reaching the cylinders ( $x/L = 0$ ). This result is similar to Maza *et al.* (2015), which obtained that the maximum turbulent intensity is not developing when the wave crest is reaching the cylinders.

Fig. 13 also shows that there is a time lag between the occurrence of maximum TKE and the maximum wave elevation of stationary cylinders, but there is no lag for swaying cylinders. That is, the maximum TKE is produced after wave crest passed each section of stationary cylinders, but it is produced as wave crest is passing each section for swaying cylinders. However, it can also be found from Fig. 14 that multiple peaks of the TKE evolution exist in the case of swaying cylinders by the return back process to its original position.

Fig. 15 shows the comparisons of vertical profile of TKE between swaying and stationary cylinders as the wave crest is passing through gauges G3 to G6. It can be seen that the strongest shear layer of both cylinders is generated near the free surface where the largest turbulence occurs, and the TKE decreases along the cylinder array. We can find that the vertical profile of TKE exists multiple shear layers due to the swaying effect of the cylinders. Fig. 15 shows the comparisons of total TKE evolution along the array of both cylinders, in which the total TKE is calculated by the integral of time evolution shown in Figs. 13 and 14. It can be found that the larger TKE occurs between  $x/L = 0.165$  and  $x/L = 0.495$  for both cylinders and the TKE of swaying cylinders is obviously less than that of stationary cylinders.

## 5. Conclusions

A numerical simulation based on the general RANS equations and RNG  $k-\varepsilon$  turbulent model was implemented to investigate the swaying effect of coastal vegetation on the damping of tsunami wave. The vegetation was idealized by a group of emergent, rigid cylinders. The FAVOR technique and general moving object (GMO) model provided in Flow-3D code were employed in this paper for simulating the coupling of fluid and rigid body interaction. The evolutions of wave height, flow field and turbulent kinetic energy for both stationary and swaying cylinder are investigated. Due to the swaying effect of the cylinders under the wave action, the numerical results showed that the damping of wave height and turbulent kinetic energy were markedly less than those of stationary cylinders. That is, tsunami damping can be overestimated if the coastal vegetation is represented as a stationary state.

## Acknowledgements

The authors would like to express their deep appreciation to Professor Maza and the anonymous reviewer for their invaluable comments and suggestions, which have led us to improve the quality of the paper.

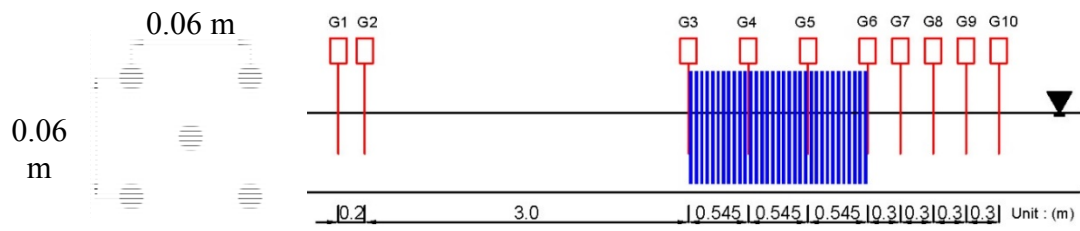
## 20 References

- Anderson, M.E., Smith, J.M., and McKay, S.K.: Wave dissipation by vegetation, Coastal and Hydraulics Engineering Technical Note ERDC/CHL CHETN-I-82, U.S. Army Engineer Research and Development Center, Vicksburg, MS., 2011.
- Augustin, L.N., Irish, J.L., and Lynett, P.: Laboratory and numerical studies of wave damping by emergent and near-emergent wetland vegetation, *Coast. Eng.*, 56, 332-340, 2009.
- Baird, A.: False hopes and natural disasters, *New York Times*, 26 December 2006.
- Bhinder, M.A., Mingham, C.G., Causon, D.M., Rahmati, M.T., Aggidis, G.A., and Chaplin, R.V.: A joint numerical and experimental study of a surging point absorbing wave energy of converter (WRASPA), *Proc. ASME 28th Inter. Conf. Ocean, Offshore and Arctic Eng.*, OMAE2009-79392, 2009.

- Choi, B.H., Kim, D.C., Pelinovsky, E., and Woo, S.B.: Three-dimensional simulation of tsunami run-up around conical island. *Coast. Eng.*, 54, 618–629, 2007.
- Cochard, R., Ranamukhaarachchi, S.L., Shivakoti, G.P., Shipin, O.V., Edwards, P.J., and Seeland, K. T. The 2004 tsunami in Aceh and Southern Thailand: A review on coastal ecosystems, wave hazards and vulnerability, *Perspectives in plant ecology, evolution and systematics*, 10(1), 3–40, 2008.
- Danielsen, F., Sorensen, M.K., Olwig, M.F., Selvam, V., Parish, F., Burgess, N.D., Hiraishi, T., Karunakaran, V. M., Rasmussen, M.S., Hansen, L.B., Quarto, A., and Suryadiputra, N.: The Asian tsunami: a protective role for coastal vegetation, *Science*, 310, 643, 2005.
- Dentale, F., Donnarumma, G., and Pugliese Carratelli, E.: Simulation of flow within armour blocks in a breakwater. *J. Coast. Res.*, 30(3), 528–536, 2014.
- Flow Science, Inc.: *Flow-3D User's Manuals*. Santa Fe, NM, 2012.
- Harada, K. and Kawata, Y.: Study on the effect of coastal forest to tsunami reduction, *Annuals of Disas. Prev. Res. Inst., Kyoto Univ.*, No. 47 C, 2004.
- Higuera, P., Lara, J.L., and Losada, I.J.: Realistic wave generation and active wave absorption for Navier–Stokes models: application to OpenFOAM, *Coast. Eng.*, 71, 102–118, 2013.
- Higuera, P., Lara, J.L., and Losada, I.J.: Three-dimensional interaction of waves and porous coastal structures using OpenFOAM. Part I: formulation and validation. *Coast. Eng.*, 83, 243–258, 2014.
- Hiraishi, T. and Harada, K.: Greenbelt tsunami prevention in south-Pacific region, *Report of the Port and Airport Research Institute*, 42 (2), 3–25, 2003.
- Hirt, C.W. and Nichols, B.D.: Volume of fluid (VOF) method for dynamics of free boundaries, *J. Comp. Phys.*, 39, 201–225, 1981.
- Hirt, C. W.: Volume-fraction techniques: powerful tools for wind engineering, *J. Wind Eng. Indust. Aerodynamics*, 46–47, 327–338, 1993.
- Huang, Z., Yao, Y., Sim, S.Y., and Yao, Y.: Interaction of solitary waves with emergent stationary vegetation, *Ocean Eng.*, 38, 1080–1088, 2011.
- Husrin, S., Strusińska, A., and Oumeraci, H.: *Experimental study on tsunami attenuation by mangrove forest*, *Earth, Planets Space*, 64, 973–989, 2012.
- Husrin, S.: *Attenuation of solitary waves and wave trains by coastal forests*, *Doctoral Thesis, TU Braunschweig, Germany*, 2013.
- Iverson, L.R. and Prasad, A.M.: Using landscape analysis to assess and model tsunami damage in Aceh province, Sumatra, *Landscape Ecol.*, 22, 323–331, 2007.
- Kazemi, A., Parry, S., van de Riet, K., and Curet, O.: The effect of porosity and flexibility on the hydrodynamics behind a mangrove-like root model, *APS Division of Fluid Dynamics (Fall) 2015*, abstract #A25.007, 2015.

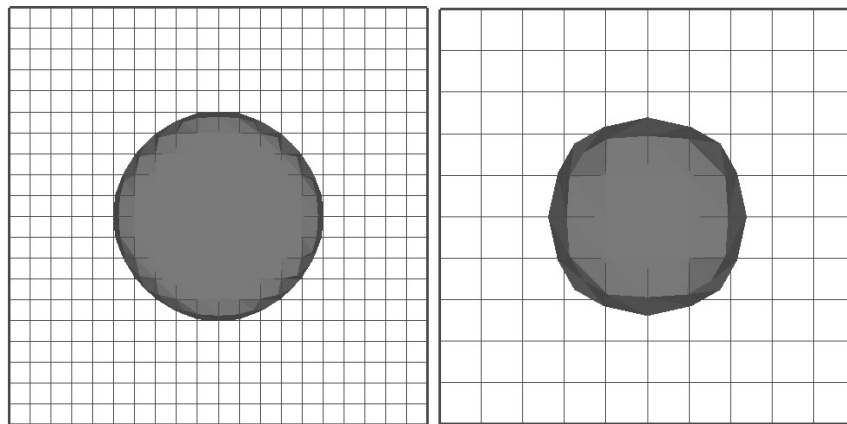
- Maza, Maria, Lara, J.L., and Losada, I.J.: Tsunami wave interaction with mangrove forests: a 3-D numerical approach, *Coast. Eng.*, 98, 33-54, 2015.
- Peltola, H., Kellomäki, S., Hassinen, A., and Granander, M.: 'Mechanical stability of Scots pine, Norway spruce and birch: an analysis of tree-pulling experiments in Finland', *Forest Ecology and Management*, 135, 143-153, 2000.
- 5 Shuto, N.: The effectiveness and limit of tsunami control forests, *Coastal Engineering in Japan*, 30, 143–153, 1987.
- Strusińska, A.; Husrin, S., and Oumeraci, H.: Tsunami damping by mangrove forest: a laboratory study using parameterized trees, *Nat. Hazards Earth Syst. Sci.*, 13, 483–503, 2013.
- Strusińska, A.; Husrin, S., and Oumeraci, H.: Attenuation of solitary wave by parameterized flexible mangrove model, *Proc. 34<sup>th</sup> Intl. Conf. Coast. Eng.*, 2014.
- 10 Teh, S.Y., Koh, H.L., Liu, P.L.F., Ismail, A.I.M., and Lee, H.L.: Analytical and numerical simulation of tsunami mitigation by mangroves in Penang, Malaysia, *J. Asian Earth Sci.*, 36, 38–46, 2009.
- Wolanski, E.: Synthesis of the protective functions of coastal forests and trees against natural hazards, *Proceedings of the regional technical workshop on Coastal protection in the aftermath of the Indian Ocean tsunami: What role for forests and trees?*, Food and Agriculture Organization of the United Nations, 2006.
- 15 Wu, W.C., Ma G., and Cox, D.T.: Modeling wave attenuation induced by the vertical density variations of vegetation, *Coast. Eng.*, 112, 17-27, 2016.
- Xiao, F.: A computational model for suspended large rigid bodies in 3D unsteady viscous flows. *J. Comput. Phys.*, 155, 348–379, 1999.
- Yakhot, V. and Orszag, S. A.: Renormalization group analysis of turbulence, I. Basic theory, *J. Sci. Comput.* 1(1), 3-51, 20 1986.
- Yakhot, V., Orszag, S.A., Thangam, S., Gatski, T.B., and Speziale, C.G.: Development of turbulence models for shear flows by a double expansion technique, *Phys. Fluids A*, 4(7), 1510-1520., 1992.
- Zhang, X, Chua, V.P., and Cheong, H.F.: Hydrodynamics in mangrove prop roots and their physical properties, *J. Hydro-environ. Res.*, 9, 281-294, 2015.
- 25 Zhao, X., Ye, Z., Fu, Y., and Cao, F.: A CIP-based numerical simulation of freak wave impact on a floating body, *Ocean Eng.*, 87, 50–63, 2014.

30



5

**Figure 1.** Cylinder cell arrangement (left), field length (right) and locations of wave probes for the computations.

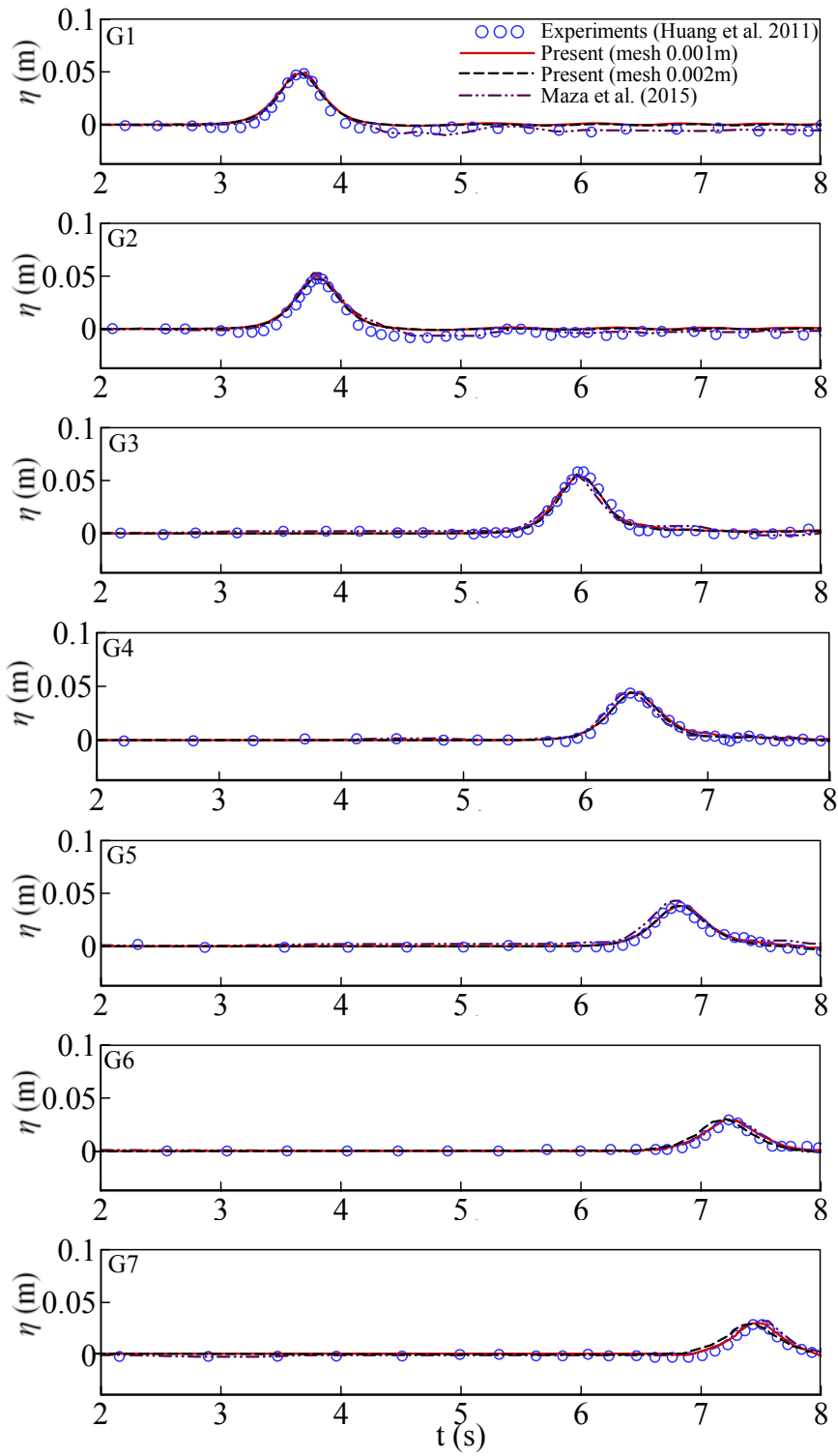


10

**Figure 2.** FAVORized geometry of cylinders and constructed computational rectangular grid with 0.001 m (left) and 0.002 m (right).

15

20



5

**Figure 3.** Comparison of free surface evolution between numerical and experimental results for  $H_i = 0.05$  m.

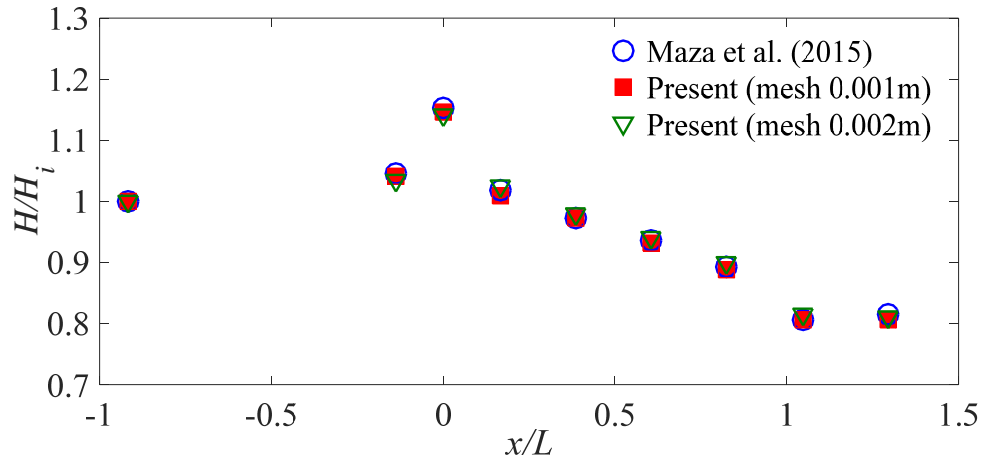


**Figure 4.** Comparison between the numerical results for the wave height for  $H_i = 0.05$  m using the field length 0.545 m.

5

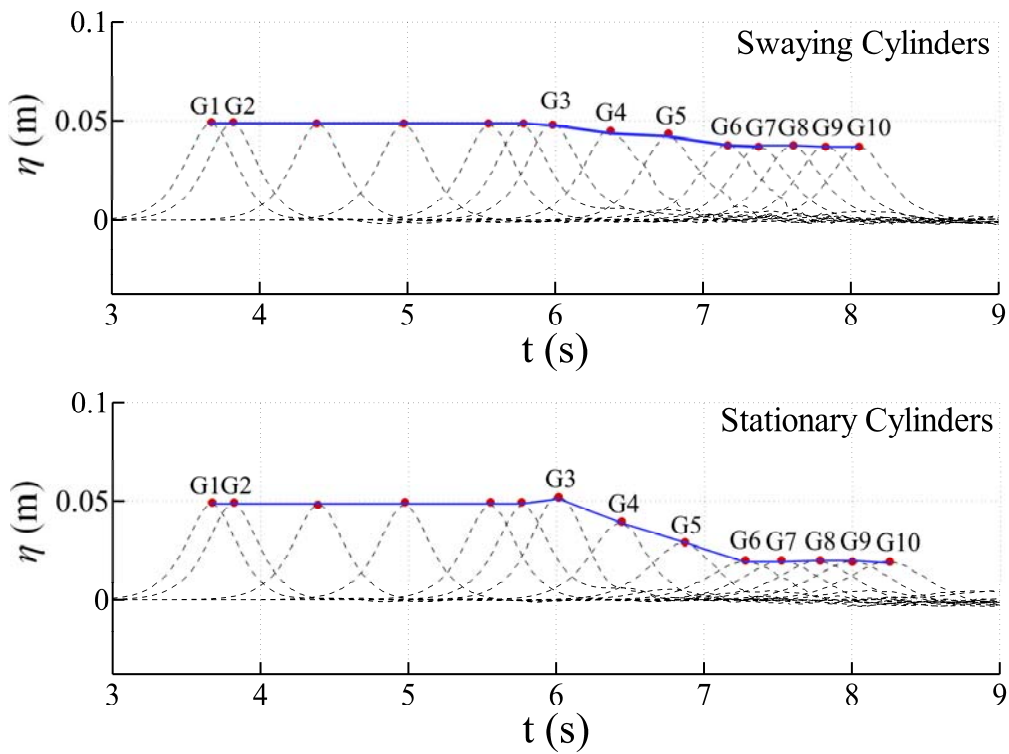


**Figure 5.** Wave surface evolutions of the swaying and stationary cylinders for an incident wave height  $H_i = 0.05$  m,  $H_i/h = 0.33$ .

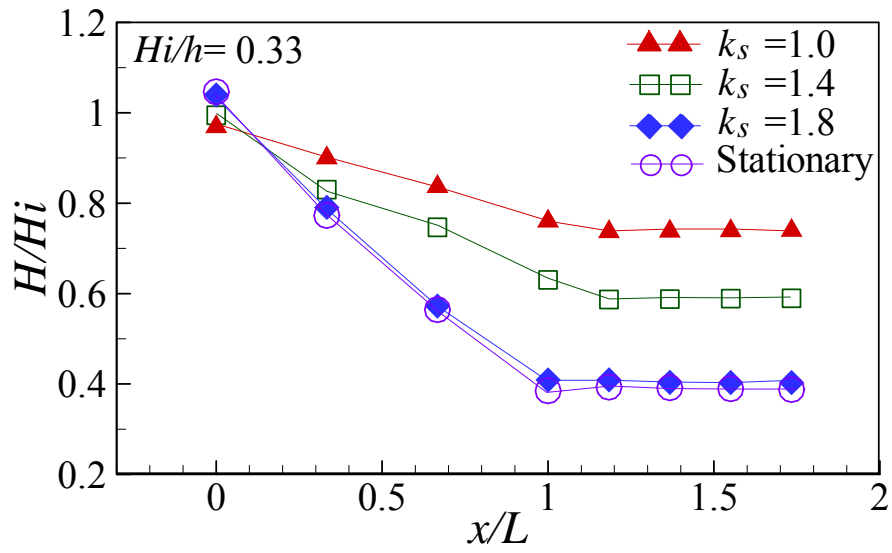


Figure 6. Comparison of wave height evolutions for swaying cylinders with different spring constants.

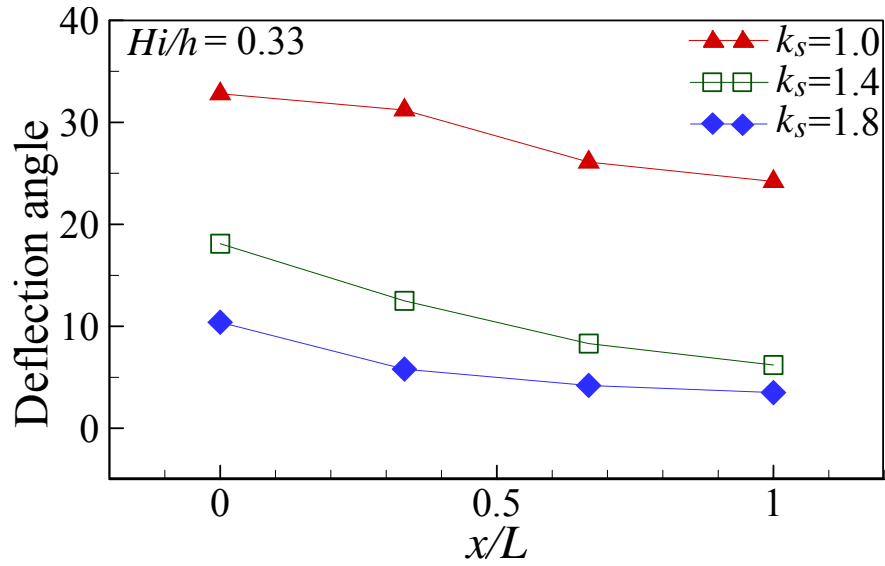
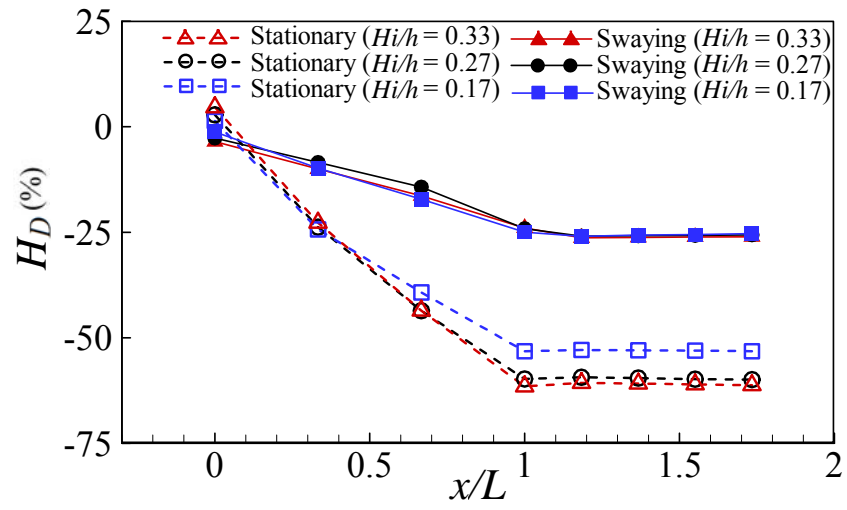


Figure 7. Comparison of the maximum deflection angles of swaying cylinders with different spring constants.

5

10



**Figure 8.** Comparison of wave height damping ratio between swaying and stationary cylinders for different incident wave heights.

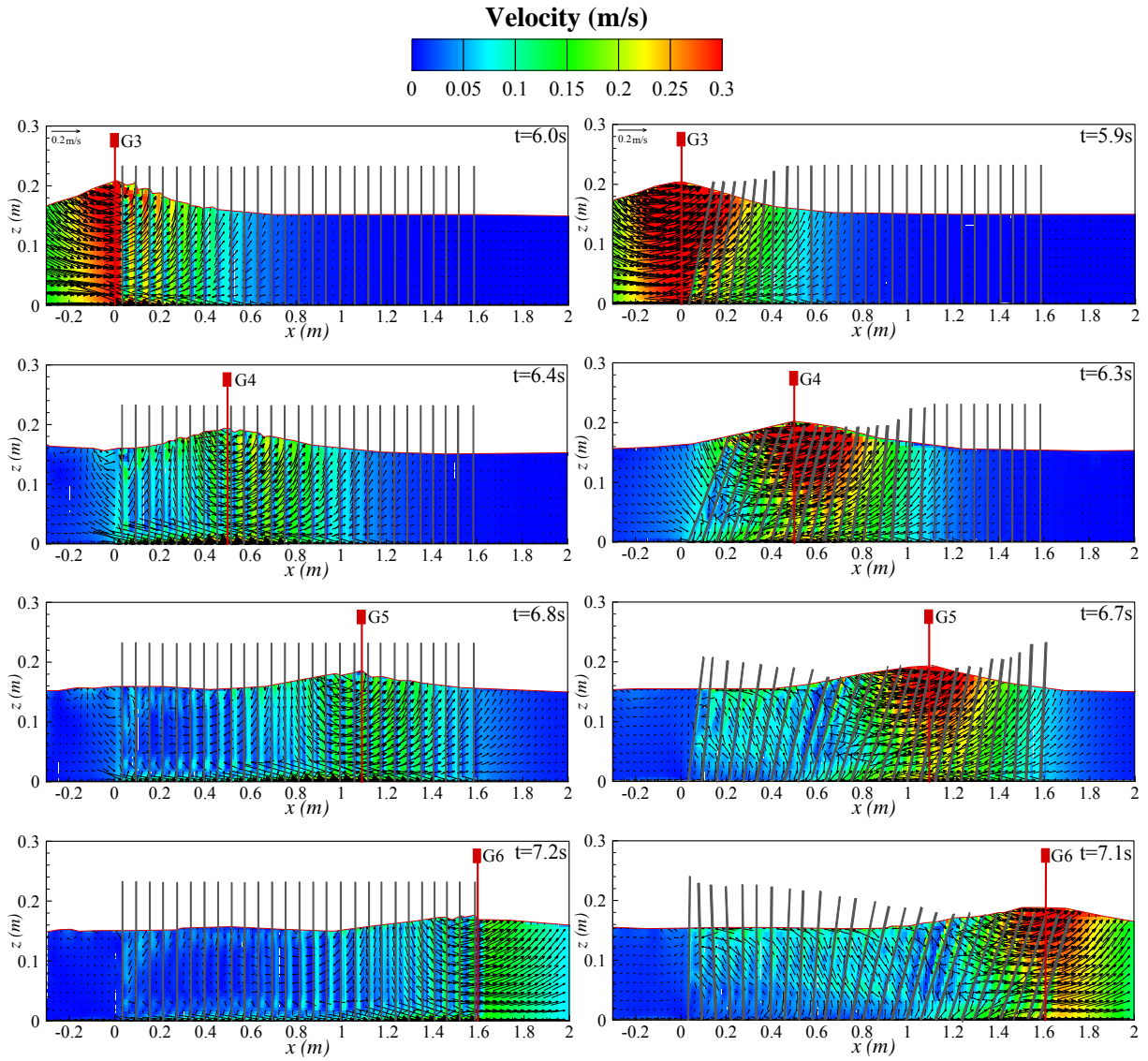


**Figure 9.** The snapshots of the velocity distribution for the stationary cylinders (left) and swaying cylinders (right) for  $H_i = 0.05$  m.

5

10

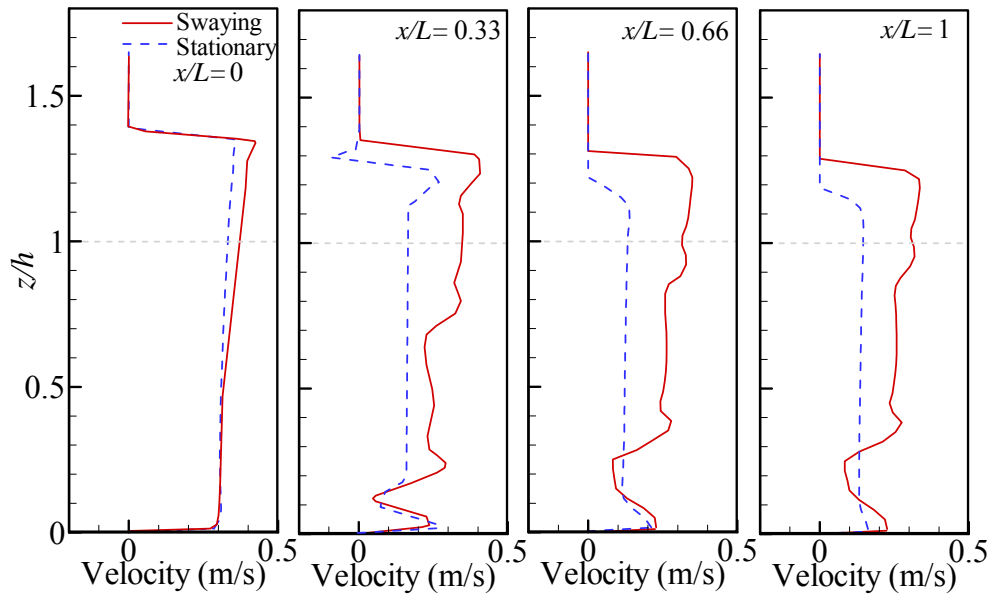


**Figure 10.** Comparison of the horizontal velocity profile for the swaying and stationary cylinders as wave crest is passing  
 5 each section for  $H_i = 0.05$  m.

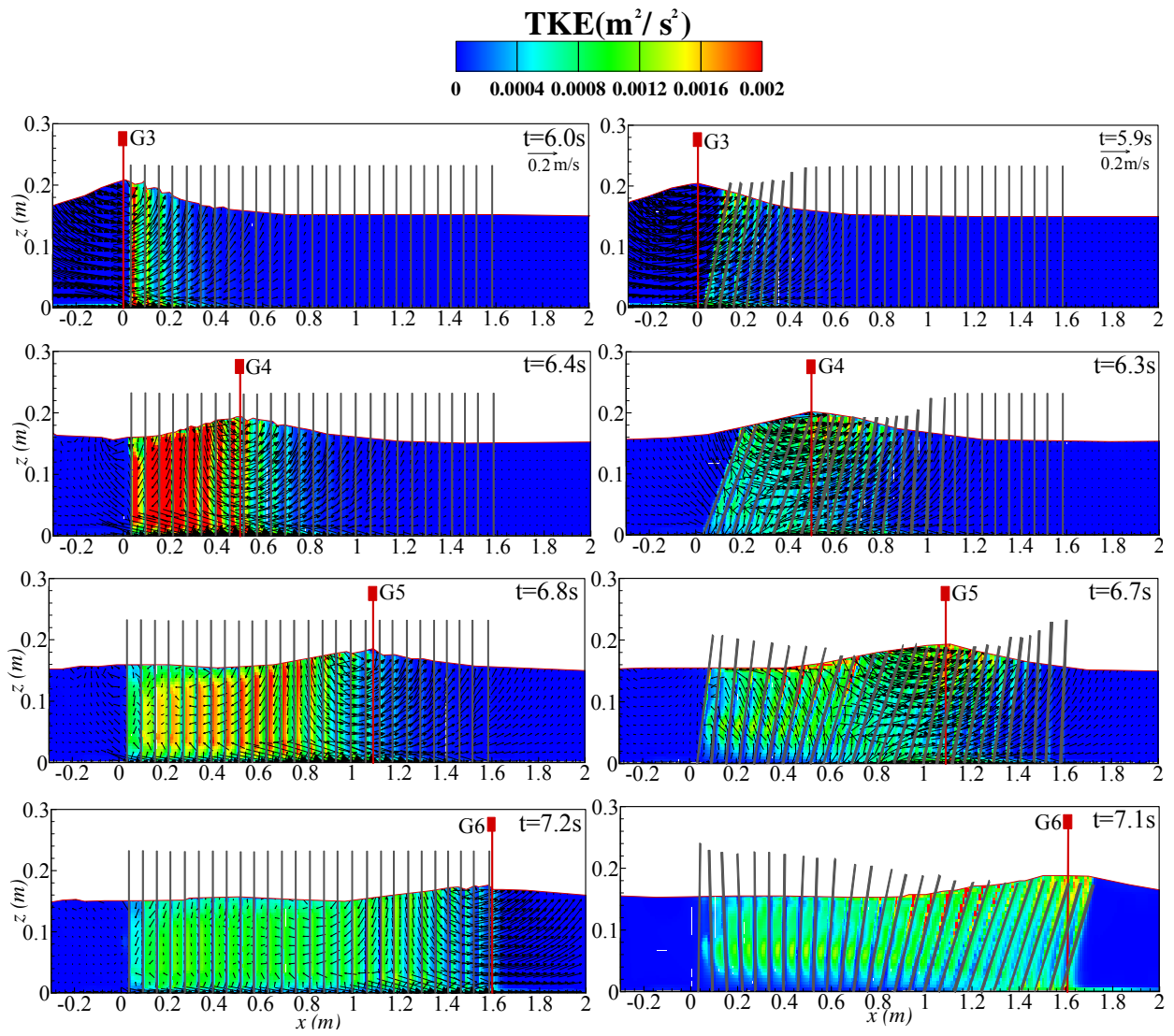


**Figure 11.** Snapshots of TKE for stationary cylinders (left) and swaying cylinders (right) for  $H_i = 0.05$  m.

DTKE ( $\text{m}^2/\text{s}^3$ )

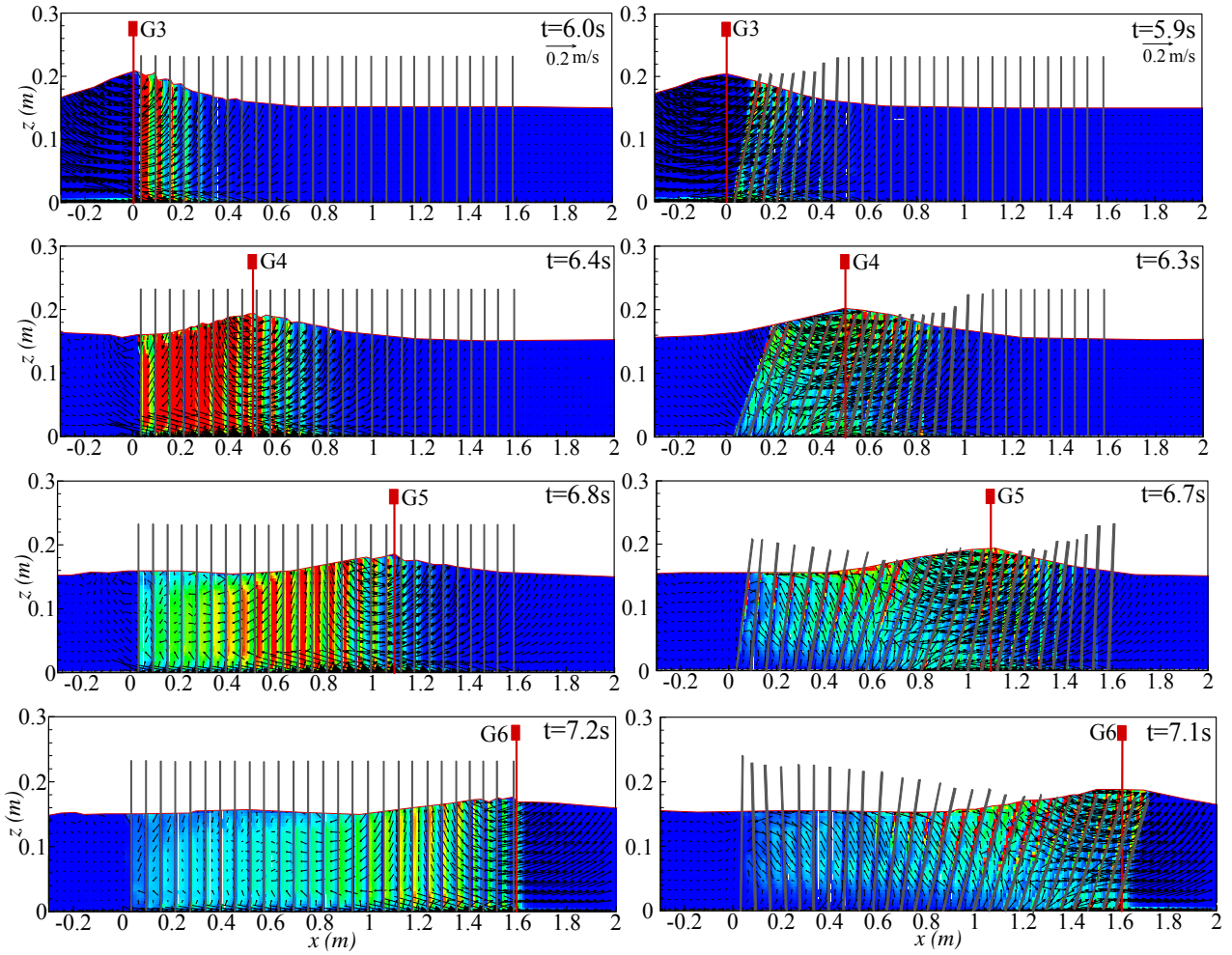


**Figure 12.** Snapshots of DTKE for stationary cylinders (left) and swaying cylinders (right) for  $H_i = 0.05$  m.

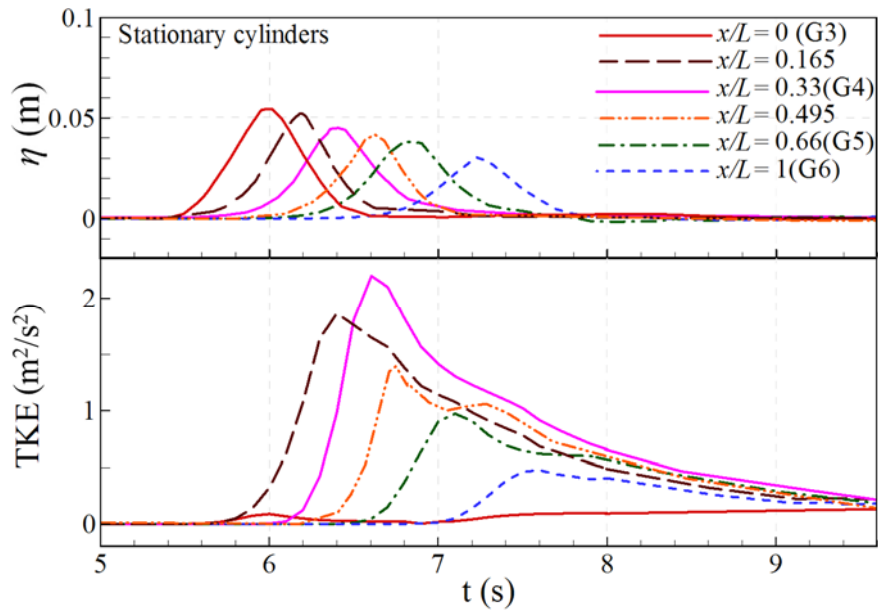


**Figure 13.** The time evolution of TKE at each section for stationary cylinders for  $H_i = 0.05$  m.

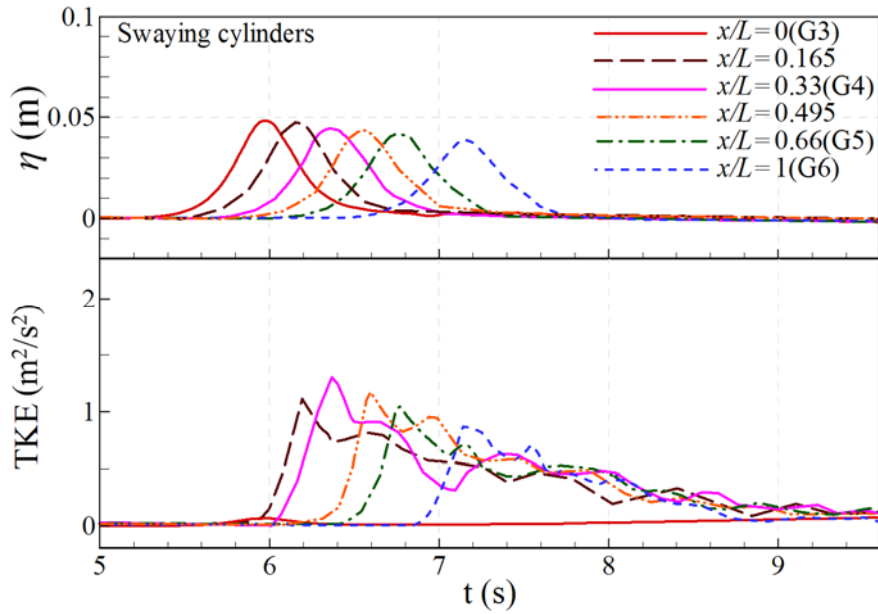


**Figure 14.** The time evolution of TKE at each section for swaying cylinders for  $H_i = 0.05$  m.

5

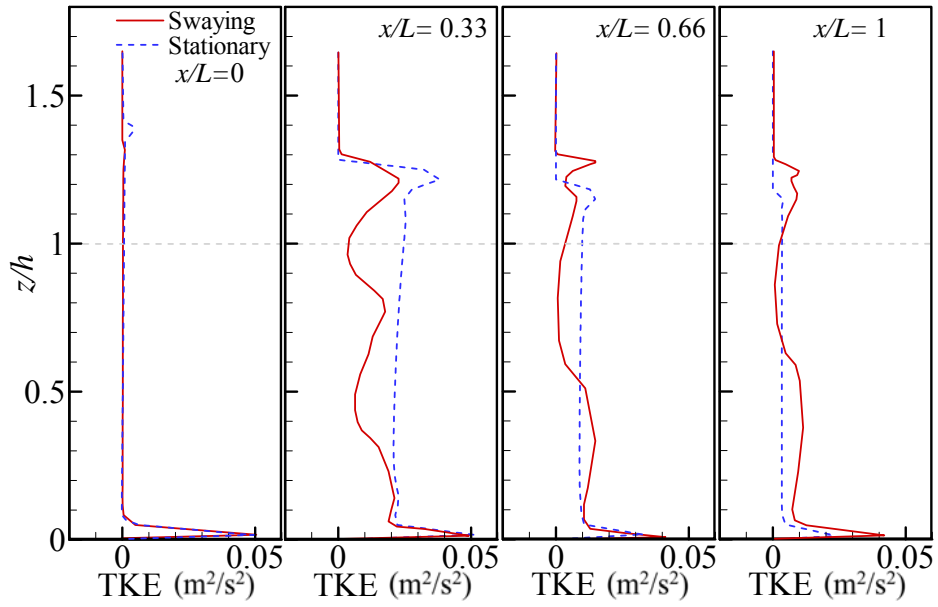


**Figure 15.** Comparison of vertical profiles of TKE as wave crest is passing through each section for  $H_i = 0.05$  m.

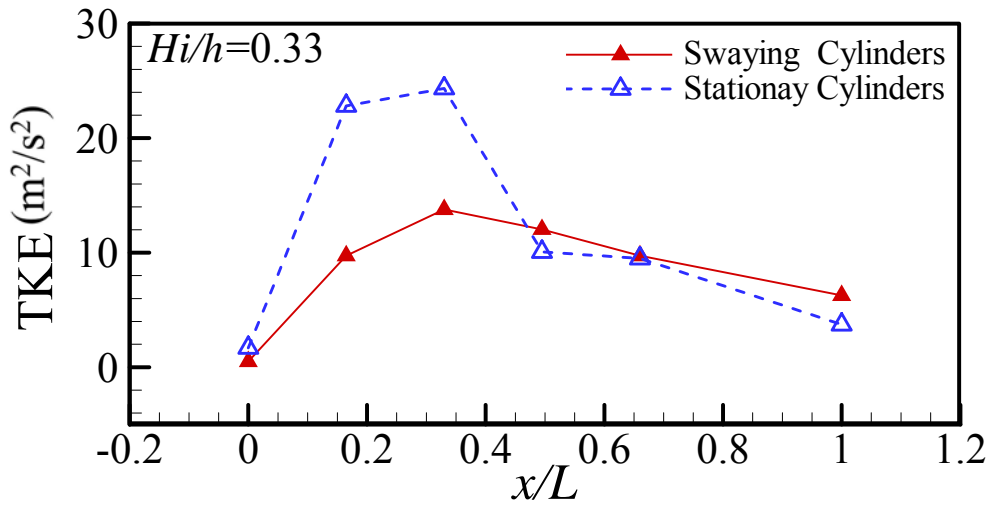


**Figure 16.** Comparison of total TKE evolution along cylinder array for  $H_i = 0.05$  m.

5